Inorganic Chemistry

Article

pubs.acs.org/IC

# Dual-Emissive Cyclometalated Iridium(III) Polypyridine Complexes as Ratiometric Biological Probes and Organelle-Selective Bioimaging Reagents

Kenneth Yin Zhang,*[,†] Hua-Wei Liu,[‡] Man-Chung Tang,[‡] Alex Wing-Tat Choi,[‡] Nianyong Zhu,[§] Xi-Guang Wei,[‡] Kai-Chung Lau,[‡] and Kenneth Kam-Wing Lo*[,‡,∥]

[†]Key Laboratory for Organic Electronics and Information Displays & Institute of Advanced Materials (IAM), Jiangsu National Synergetic Innovation Center for Advanced Materials (SICAM), Nanjing University of Posts & Telecommunications, 9 Wenyuan Road, Nanjing 210023, P. R. China

[‡]Department of Biology and Chemistry, City University of Hong Kong, Tat Chee Avenue, Kowloon, Hong Kong, P. R. China

[§]Department of Chemistry, The University of Hong Kong, Pokfulam Road, Hong Kong, P. R. China

[∥]State Key Laboratory of Millimeters Waves, City University of Hong Kong, Tat Chee Avenue, Kowloon, Hong Kong, P. R. China

Supporting Information

**ABSTRACT:** In this Article, we present a series of cyclometalated iridium(III) polypyridine complexes of the formula $[Ir(N^C)_2(N^N)](PF_6)$ that showed dual emission under ambient conditions. The structures of the cyclometalating and diimine ligands were changed systematically to investigate the effects of the substituents on the dual-emission properties of the complexes. On the basis of the photophysical data, the high-energy (HE) and low-energy (LE) emission features of the complexes were assigned to triplet intraligand ($^3$IL) and triplet charge-transfer ($^3$CT) excited states, respectively. Time-dependent density functional theory (TD-DFT) calculations supported these assignments and indicated that the dual emission resulted from the interruption of the communication between the higher-lying $^3$IL and the lower-lying $^3$CT states by a triplet amine-to-ligand charge-transfer ($^3$NLCT) state. Also, the avidin-binding properties of the biotin complexes were studied by emission titrations, and the results showed that the dual-emissive complexes can be utilized as ratiometric probes for avidin. Additionally, all the complexes exhibited efficient cellular uptake by live HeLa cells. The MTT and Annexin V assays confirmed that no cell death and early apoptosis occurred during the cell imaging experiments. Interestingly, laser-scanning confocal microscopy revealed that the complexes were selectively localized on the cell membrane, mitochondria, or both, depending on the nature of the substituents of the ligands. The results of this work will contribute to the future development of dual-emissive transition metal complexes as ratiometric probes and organelle-selective bioimaging reagents.

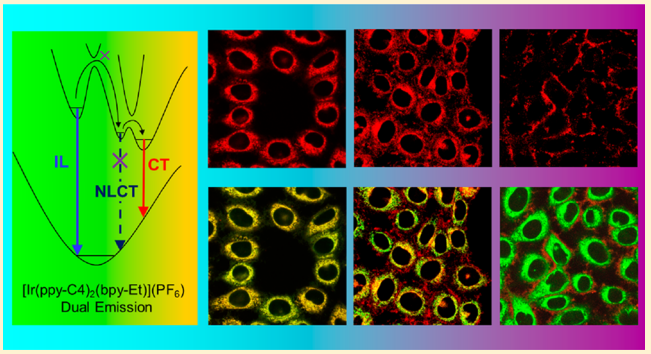


## INTRODUCTION

Due to the high sensitivity and short response time of fluorescence sensing, there has been much interest in using fluorescent materials including organic dyes,[1−6] transition metal complexes,[5−10] lanthanide chelates,[5,6,11] and inorganic nanoparticles[12,13] as probes for environmental physical parameters and chemical analytes. Fluorescent probes have been applied to visualize live cells[13−20] and measure intracellular temperature,[21] oxygen content,[22] pH,[23] and the concentration of metal cations[24−27] and various endogenous analytes[28−31] by laser-scanning confocal microscopy. However, the results of fluorescence intensity-based sensing may be easily affected by the inherent variability in incident laser power and intracellular concentration of the probe itself. An alternative approach involving dual-emissive probes that display a change in the ratio of the two emission bands will enable self-calibration of the fluorescence signals and hence more accurate quantification of the analyte. The current design of dual-emissive probes relies on covalent connection or hybridization of two fluorescent compounds.[32−36] Although it is a straightforward strategy, there are some limitations: for example, (1) a complicated synthetic process is required to put the two units together, (2) the resultant probes usually have a large molecular size, which reduces their cellular uptake efficiency, and (3) possible electron- and/or energy-transfer between the two fluorescent units may lower the accuracy of the sensing. Thus, simple dual-emissive compounds with single-wavelength excitation are

Received: April 27, 2015





DOI: 10.1021/acs.inorgchem.5b00944
Inorg. Chem. XXXX, XXX, XXX−XXX

more attractive candidates because these potential problems can be avoided. Although Kasha's rule states that fluorescence only occurs from the lowest-energy excited state,[37] transition metal complexes that simultaneously display dual emission from two excited states under ambient conditions have been reported.[38−40] For example, charge-neutral iridium(III) complexes exhibiting dual emission have been used as a ratiometric sensor for the $Cu^{2+}$ ion.[40] Since cationic complexes enter live cells more readily than neutral ones,[41−44] we anticipate that cationic dual-emissive systems will afford intracellular ratiometric probes with high cellular uptake efficiency.

Previously, we have discovered a cationic cyclometalated iridium(III) polypyridine complex with an amine on the cyclometalating ligand and an amide on the diimine ligand $[Ir(ppy\text{-}C4)_2(bpy\text{-}Et)](PF_6)$ (Hppy-C4 = 2-(4-((*N*-*n*-butyl)-aminomethyl)phenyl)pyridine, bpy-Et = 4-(*N*-(ethyl)-aminocarbonyl)-4′-methyl-2,2′-bipyridine) that displays interesting dual emission under ambient conditions.[45] Remarkably, the high-energy (HE) and low-energy (LE) emission features, and hence the overall emission profile, depend strongly on the polarity of the local environment of the complex. The complex has also been derivatized to afford homogeneous sensors for avidin, estrogen receptor $\alpha$, and lipid-binding proteins. To rationalize the roles of the amine and ligand structures in the dual-emission properties of these complexes, and to understand the effects of the ligands on their cellular uptake and intracellular localization properties, we have launched a program to design new dual-emissive cyclometalated iridium(III) polypyridine complexes and examine their photophysical and biological properties. Herein we report the synthesis and characterization of a family of structurally related complexes $[Ir(N^C)_2(N^N)](PF_6)$ (HN^C = Hppy-C4, 2-((4′-((*N*-*n*-butyl)aminomethyl)-1,1′-biphenyl)-4-yl)pyridine (Hpppy-C4); N^N = bpy-Et, 3,4,7,8-tetramethyl-1,10-phenanthroline ($Me_4$-phen), 4,4′-dimethyl-2,2′-bipyridine ($Me_2$-bpy), 1,10-phenanthroline (phen), 4,7-diphenyl-1,10-phenanthroline ($Ph_2$-phen)) (Chart 1). Also, complexes without the amine groups $[Ir(pppy)_2(N^N)](PF_6)$ (Hpppy = 2-((1,1′-biphenyl)-4-yl)-pyridine, N^N = bpy-Et, $Me_4$-phen, $Me_2$-bpy, phen, $Ph_2$-phen) were synthesized for comparison studies. Additionally, time-dependent density functional theory (TD-DFT) calculations were performed on $[Ir(ppy)_2(bpy\text{-}Et)](PF_6)$ (Hppy = 2-phenylpyridine) and $[Ir(ppy\text{-}C4)_2(bpy\text{-}Et)](PF_6)$ to understand their excited-state nature. With an aim to evaluate the potential application of these complexes as ratiometric probes, we incorporated biotin into the dual-emissive system, affording the complexes $[Ir(N^C)_2(bpy\text{-}biotin)](PF_6)$ (HN^C = Hppy-C4, Hpppy-C4, Hpppy) (Chart 1) as luminescent probes for avidin. Furthermore, the cellular uptake efficiency and live cell staining properties of these complexes were studied using human cervix epithelioid carcinoma (HeLa) cells as a model cell line. The MTT (3-(4,5-dimethyl-2-thiazolyl)-2,5-diphenyl-tetrazolium bromide) and Annexin V assays were performed to determine the optimal conditions for live cell imaging, under which images of good quality can be obtained with minimum cell death. Furthermore, the intracellular localization of all the complexes was investigated by laser-scanning confocal microscopy, and the specific organelle staining was also confirmed by co-staining experiments.

## RESULTS AND DISCUSSION

**Synthesis and Characterization.** Regarding the design of our ligands, an additional phenyl ring was incorporated into the ppy-C4 ligand yielding the pppy-C4 ligand to study the effects of the cyclometalating ligands. The importance of the amine group was investigated using the pppy ligand as an amine-free analogue for pppy-C4. Also, five diimine ligands were selected to elucidate the role of the $\pi^*$(N^N) orbitals on the dual-emission properties of the complexes. The cyclometalating ligands 2-((4′-formyl-1,1′-biphenyl)-4-yl)pyridine (Hpppy-CHO) and Hpppy were synthesized by the Suzuki coupling of 2-(4-bromophenyl)pyridine with 4-formylphenylboronic acid and phenylboronic acid, respectively, using $Pd(PPh_3)_2Cl_2$ as the catalyst (Scheme 1).[46] The cyclometalated iridium(III) polypyridine complexes $[Ir(N^C)_2(N^N)](PF_6)$ (HN^C = 4-(2-pyridyl)benzaldehyde (Hppy-CHO), Hpppy-CHO, Hpppy) were obtained from the reaction of the dichloro-bridged dimer $[Ir_2(N^C)_4Cl_2]$ with the diimine ligand N^N in refluxing $CH_2Cl_2$/MeOH. During the preparation of the aldehyde complexes $[Ir(pppy\text{-}CHO)_2(N^N)](PF_6)$, we found that the aldehyde groups reacted with MeOH in the solvent mixture and formed stable acetals. To avoid this, a mixture of MeOH/$CH_2Cl_2$/$H_2O$ (1:3:1, v/v) was used as the solvent for the reaction. The amine-containing complexes $[Ir(ppy\text{-}C4)_2(N^N)](PF_6)$ and $[Ir(pppy\text{-}C4)_2(N^N)](PF_6)$ were synthesized from the reductive amination of their respective aldehyde precursor complexes $[Ir(ppy\text{-}CHO)_2(N^N)](PF_6)$ and $[Ir(pppy\text{-}CHO)_2(N^N)](PF_6)$ with *n*-butylamine. All the complexes were characterized by $^1H$ NMR spectroscopy, IR spectroscopy, positive-ion ESI-MS, elemental microanalysis, UV−vis absorption spectroscopy, and cyclic voltammetry.

The complexes exhibited good solubility in common organic solvents and aqueous MeOH or DMSO solutions except $[Ir(pppy\text{-}C4)_2(bpy\text{-}biotin)](PF_6)$, which was almost insoluble in $CH_2Cl_2$, and $[Ir(pppy)_2(N^N)](PF_6)$ (N^N = $Me_4$-phen, $Me_2$-bpy, phen, $Ph_2$-phen), which were sparingly soluble in aqueous buffers containing as much as 50% MeOH or DMSO.

**Chart 1. Structures of the Complexes**

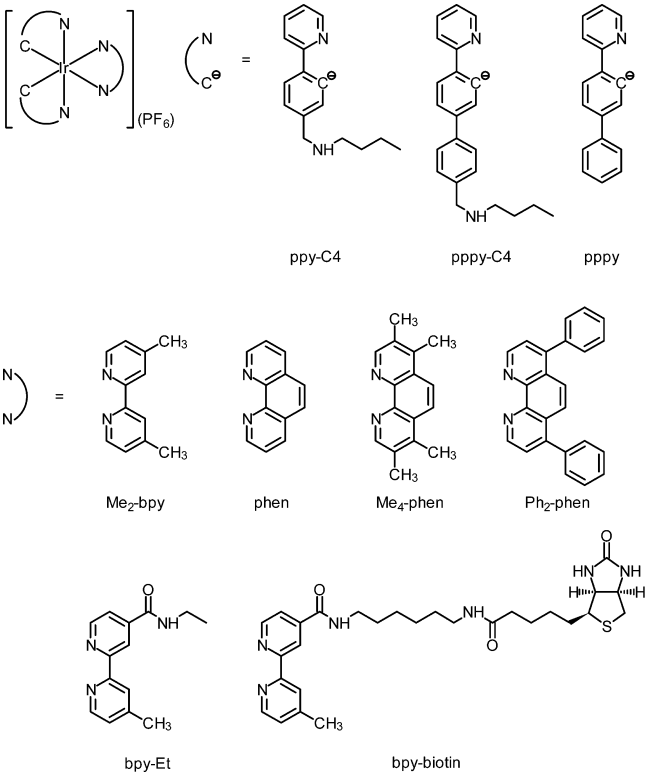



DOI: 10.1021/acs.inorgchem.5b00944
*Inorg. Chem.* XXXX, XXX, XXX−XXX

**Scheme 1. Synthetic Procedure of the Cyclometalating Ligands Hpppy-CHO and Hpppy**

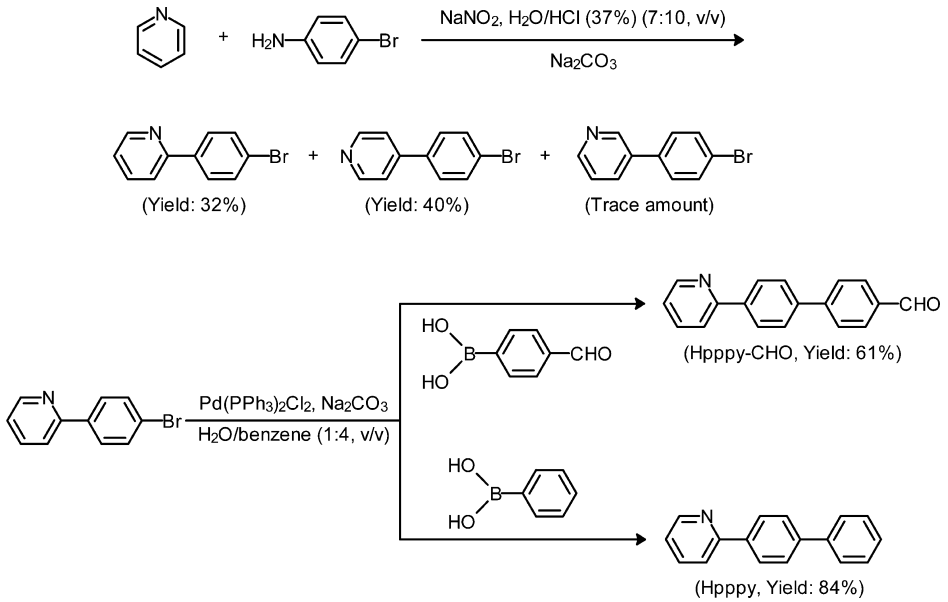


Single crystals of $[Ir(ppy\text{-}C4)_2(Me_2\text{-}bpy)](PF_6)$ suitable for X-ray crystallographic studies were obtained by layering petroleum ether (40−60 °C) over a concentrated acetone solution of the complex. The perspective view of complex cation $[Ir(ppy\text{-}C4)_2(Me_2\text{-}bpy)]^+$ with the atomic numbering scheme is depicted in Figure 1. Selected bond lengths and bond angles are listed in Supporting Information Table S1. Similar to related bis(cyclometalated) iridium(III) polypyridine complexes,[18] the iridium(III) center of $[Ir(ppy\text{-}C4)_2(Me_2\text{-}bpy)]^+$ adopted a distorted octahedral geometry, and the *trans* angles at the metal center ranged from 171.85(17)° to 174.2(2)°. The metal−carbon bonds around the iridium(III) center were in a *cis* orientation, and the bond lengths were 2.022(5) Å. As expected, the *trans*-influence of the carbon donors rendered longer Ir−N bond lengths for the $Me_2$-bpy ligand (2.159(4) Å) than the ppy-C4 ligands (2.057(5) Å). The bite angles of the ppy-C4 ligands (80.6(2)°) were larger than that of the $Me_2$-bpy ligand (76.0(2)°).

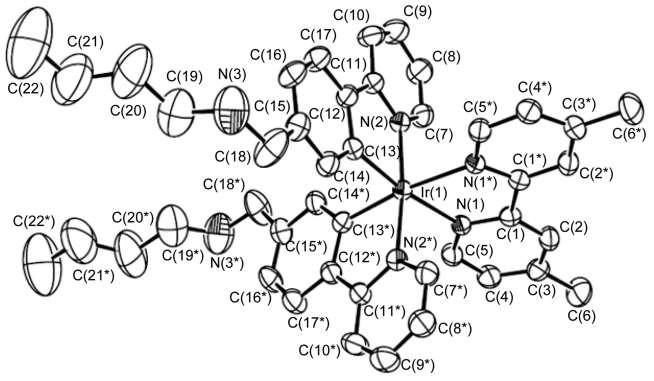


**Figure 1.** Perspective view of the complex cation $[Ir(ppy\text{-}C4)_2(Me_2\text{-}bpy)]^+$ with the atomic numbering scheme. Thermal ellipsoids are shown at the 30% probability level. Hydrogen atoms are omitted for clarity.

**Electronic Absorption and Electrochemical Properties.** The electronic absorption spectral data of the iridium(III) complexes in selected solvents at 298 K are listed in Supporting Information Table S2. All the complexes showed intense spin-allowed $^1$IL ($\pi \rightarrow \pi^*$) (N^N and N^C) absorption bands and shoulders in the UV region and less intense absorption features related to spin-allowed metal-to-ligand charge-transfer ($^1$MLCT) ($d\pi(Ir) \rightarrow \pi^*$(N^N and N^C)) transitions in the visible region. The pppy-C4 complexes revealed stronger absorption at ca. 250−325 nm than their pppy counterparts, probably due to additional singlet amine-to-ligand charge-transfer ($^1$NLCT) (amine $\rightarrow \pi^*$(N^N and N^C)) transitions (Supporting Information Table S2 and Figure S1). The electrochemical properties of the iridium(III) complexes were studied by cyclic voltammetry, and the electrochemical data are listed in Supporting Information Table S3. The amine-containing ppy-C4 and pppy-C4 complexes exhibited two oxidation processes: an irreversible wave at +0.87 to +1.15 V and a quasireversible couple at +1.24 to +1.46 V versus SCE, which were assigned to the oxidation of the secondary amine groups and the iridium center, respectively. The amine-free pppy complexes only showed one reversible iridium(IV/III) oxidation couple at +1.22 to +1.27 V. The first reduction couples of the diimine ligands of all the complexes were reversible in nature and appeared at ca. −1.23 to −1.63 V versus SCE.

**Emission Properties.** Upon photoexcitation, all the complexes exhibited intense and long-lived green to orange luminescence in degassed fluid solutions under ambient conditions. The photophysical data of the complexes are summarized in Table 1. The emission properties of these complexes are highly dependent on both cyclometalating and diimine ligands. First, the effects of the cyclometalating ligands on the emission properties were investigated using the complexes $[Ir(N^C)_2(bpy\text{-}Et)](PF_6)$ (N^C = ppy-C4, pppy-C4, ppy, pppy) as examples. Interestingly, the amine-containing ppy-C4 and pppy-C4 complexes showed well-resolved dual emission that was composed of a vibronically structured high-energy (HE) emission feature in blue-green region and a structureless low-energy (LE) emission band in the yellow to orange-red region (Figure 2a,b, Table 1). The emission colors of these two complexes depended on the polarity of the solvents. In less polar $CH_2Cl_2$, the HE emission intensity was


DOI: 10.1021/acs.inorgchem.5b00944
*Inorg. Chem.* XXXX, XXX, XXX−XXX

**Table 1. Photophysical Data of the Complexes in Deaerated Solutions**

| complex | medium ($T$/K) | $\lambda_{em}$/nm | $\tau_o$/$\mu$s | $\Phi_{em}$ |
|---|---|---|---|---|
| [Ir(ppy-C4)$_2$(bpy-Et)](PF$_6$) | $CH_2Cl_2$ (298) | 498 sh, 521 | 1.06 | 0.11 |
| | | 593 (max) | 0.28 | |
| | $CH_3CN$ (298) | 495, 523 sh | 1.43 | 0.065 |
| | | 612 sh | 0.14 | |
| | buffer[a] (298) | 500, 525 sh | 2.48 | 0.17 |
| [Ir(pppy-C4)$_2$(bpy-Et)](PF$_6$) | $CH_2Cl_2$ (298) | 531, 576 sh | 4.37 | 0.18 |
| | | 602 (max) | 0.55 | |
| | $CH_3CN$ (298) | 528, 573 sh | 4.73 | 0.079 |
| | | 604 (max) | 0.30 | |
| | buffer[a] (298) | 528 (max), 563 | 6.52 | 0.14 |
| | | 606 sh | 0.052 | |
| [Ir(ppy)$_2$(bpy-Et)](PF$_6$) | $CH_2Cl_2$ (298) | 609 | 0.40 | 0.13 |
| | $CH_3CN$ (298) | 613 | 0.23 | 0.058 |
| | buffer[b] (298) | 626 | 0.078 | 0.0069 |
| [Ir(pppy)$_2$(bpy-Et)](PF$_6$) | $CH_2Cl_2$ (298) | 598 | 0.46 | 0.13 |
| | $CH_3CN$ (298) | 602 | 0.27 | 0.069 |
| | buffer[a] (298) | 608 | 0.041 | [c] |
| [Ir(ppy-C4)$_2$(Me$_4$-phen)](PF$_6$) | $CH_2Cl_2$ (298) | 482 sh | 2.56 | 0.47 |
| | | 518 | 1.82 | |
| | $CH_3CN$ (298) | 482 sh | 2.49 | 0.43 |
| | | 538 | 1.58 | |
| | buffer[a] (298) | 482 (max), 512, 556 sh | 4.45 | 0.46 |
| [Ir(ppy-C4)$_2$(Me$_2$-bpy)](PF$_6$) | $CH_2Cl_2$ (298) | 487 sh | 1.98 | 0.39 |
| | | 559 | 0.73 | |
| | $CH_3CN$ (298) | 484 sh | 1.46 | 0.23 |
| | | 565 | 0.39 | |
| | buffer[a] (298) | 490, 518 (max) | 2.41 | 0.15 |
| | | 576 sh | 0.30 | |
| [Ir(ppy-C4)$_2$(phen)](PF$_6$) | $CH_2Cl_2$ (298) | 577 | 0.84 | 0.41 |
| | $CH_3CN$ (298) | 584 | 0.51 | 0.25 |
| | buffer[a] (298) | 480 sh | 2.92 | 0.10 |
| | | 566 | 0.35 | |
| [Ir(ppy-C4)$_2$(Ph$_2$-phen)](PF$_6$) | $CH_2Cl_2$ (298) | 579 | 0.93 | 0.40 |
| | $CH_3CN$ (298) | 580 | 0.53 | 0.26 |
| | buffer[a] (298) | 577 | 0.37 | 0.12 |
| [Ir(pppy-C4)$_2$(Me$_4$-phen)](PF$_6$) | $CH_2Cl_2$ (298) | 522 (max), 552, 606 sh | 1.02 | 0.48 |
| | $CH_3CN$ (298) | 520 (max), 550, 604 sh | 6.80 | 0.42 |
| | buffer[a] (298) | 520 (max), 552, 602 sh | 10.00 | 0.40 |
| [Ir(pppy-C4)$_2$(Me$_2$-bpy)](PF$_6$) | $CH_2Cl_2$ (298) | 524 sh, 553 | 1.33 | 0.44 |
| | $CH_3CN$ (298) | 524 sh, 556 | 1.58 | 0.23 |
| | buffer[a] (298) | 523 (max), 557, 619 sh | 2.97 | 0.12 |
| [Ir(pppy-C4)$_2$(phen)](PF$_6$) | $CH_2Cl_2$ (298) | 561 | 1.17 | 0.45 |
| | $CH_3CN$ (298) | 567 | 1.11 | 0.23 |
| | buffer[a] (298) | 523 sh, 558 | 1.44 | 0.09 |
| [Ir(pppy-C4)$_2$(Ph$_2$-phen)](PF$_6$) | $CH_2Cl_2$ (298) | 567 | 1.12 | 0.50 |
| | $CH_3CN$ (298) | 577 | 0.91 | 0.23 |
| | buffer[a] (298) | 575 | 2.03 | 0.08 |
| [Ir(pppy)$_2$(Me$_4$-phen)](PF$_6$) | $CH_2Cl_2$ (298) | 523 (max), 551, 603 sh | 8.62 | 0.46 |
| | $CH_3CN$ (298) | 521 (max), 551, 601 sh | 7.31 | 0.41 |
| | buffer[a] (298) | 516 (max), 551, 601 sh | 5.61 | [c] |
| [Ir(pppy)$_2$(Me$_2$-bpy)](PF$_6$) | $CH_2Cl_2$ (298) | 522 sh, 555 | 1.22 | 0.44 |
| | $CH_3CN$ (298) | 526 sh, 560 | 1.12 | 0.28 |
| | buffer[a] (298) | 525 sh, 554 | 0.47 | [c] |
| [Ir(pppy)$_2$(phen)](PF$_6$) | $CH_2Cl_2$ (298) | 564 | 1.19 | 0.42 |
| | $CH_3CN$ (298) | 569 | 1.06 | 0.28 |
| | buffer[a] (298) | 562 | 0.36 | [c] |
| [Ir(pppy)$_2$(Ph$_2$-phen)](PF$_6$) | $CH_2Cl_2$ (298) | 571 | 1.07 | 0.51 |
| | $CH_3CN$ (298) | 578 | 0.96 | 0.45 |
| | buffer[a] (298) | 562 | 0.39 | [c] |
| [Ir(ppy-C4)$_2$(bpy-biotin)](PF$_6$) | $CH_2Cl_2$ (298) | 494 (max), 523 | 1.92 | 0.24 |
| | | 574 | 0.57 | |
| | $CH_3CN$ (298) | 492, 518 sh | 2.06 | 0.11 |
| | | 601 sh | 0.34 | |
| | buffer[a] (298) | 492, 517 sh | 2.61 | 0.13 |
| [Ir(pppy-C4)$_2$(bpy-biotin)](PF$_6$) | $CH_2Cl_2$ (298) | 526 sh | 4.57 | 0.15 |
| | | 589 | 0.44 | |
| | MeOH (298) | 528, 574 sh | 5.48 | 0.051 |
| | | 602 (max) | 0.15 | |
| | buffer[a] (298) | 528 (max), 567 | 7.03 | 0.10 |
| | | 612 sh | 0.065 | |
| [Ir(pppy)$_2$(bpy-biotin)](PF$_6$) | $CH_2Cl_2$ (298) | 590 | 0.50 | 0.17 |
| | $CH_3CN$ (298) | 601 | 0.28 | 0.074 |
| | buffer[b] (298) | 611 | 0.051 | [c] |

[a] 50 mM potassium phosphate buffer pH 7.4/DMSO (7:3, v/v). [b] 50 mM potassium phosphate buffer pH 7.4/MeOH (3:7, v/v). [c] The quantum yield cannot be determined accurately due to insufficient solubility of the complex.



DOI: 10.1021/acs.inorgchem.5b00944
Inorg. Chem. XXXX, XXX, XXX−XXX

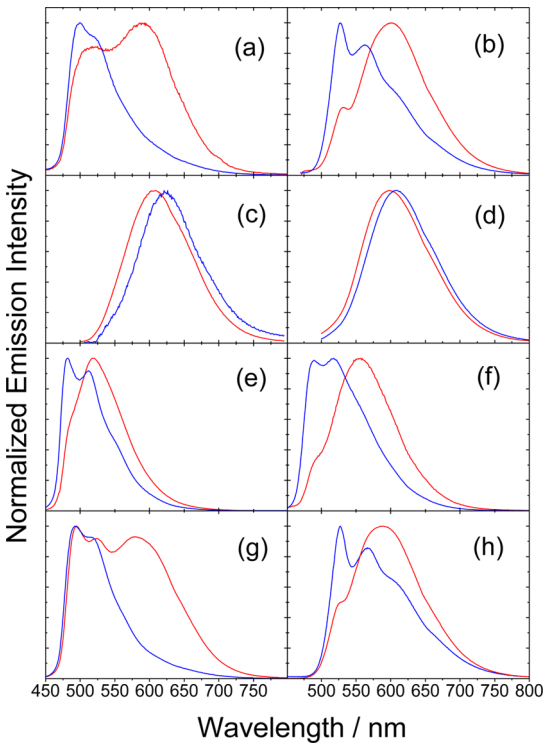


**Figure 2.** Emission spectra of $[Ir(N^C)_2(bpy\text{-}Et)](PF_6)$ (N^N = ppy-C4 (a), pppy-C4 (b), ppy (c), pppy (d)), $[Ir(ppy\text{-}C4)_2(N^N)](PF_6)$ (N^N = $Me_4$-phen (e), $Me_2$-bpy (f)), and $[Ir(ppy\text{-}C4)_2(bpy\text{-}biotin)](PF_6)$ (g) in deaerated $CH_2Cl_2$ (red) and potassium phosphate buffer (blue) at 298 K. (h) Emission spectra of $[Ir(pppy\text{-}C4)_2(bpy\text{-}biotin)](PF_6)$ in deaerated $CH_3CN$ (red) and potassium phosphate buffer (blue) at 298 K.

lower than that of the LE band, and the emission was orange in color. In more polar $CH_3CN$, the LE emission intensity was reduced. In aqueous buffer, the emission spectra were dominated by the HE band, and the LE emission was completely embedded or appeared as an unresolved shoulder, giving green and yellow emission. The lifetimes of both emission bands were in the microsecond or submicrosecond time scales, indicative of triplet-state nature. Additionally, upon increasing the polarity of the solvent, the lifetimes of the HE emission were extended whereas those of the LE emission were shortened. With the change in the cyclometalating ligand from ppy-C4 to pppy-C4, the HE emission was shifted to a longer wavelength by ca. 30 nm with increased lifetimes, whereas the low-energy emission wavelength was less affected (Figure 2a,b). On the basis of these photophysical data, we assigned the HE band of the complexes to a triplet intraligand $^3$IL ($\pi \rightarrow \pi^*$) (N^C) excited state and the LE feature to a triplet charge-transfer ($^3$CT) excited state of mixed $^3$MLCT ($d\pi(Ir) \rightarrow \pi^*$(bpy-Et)) and $^3$LLCT ($\pi$(N^C) $\rightarrow \pi^*$(bpy-Et)) character. Additionally, the dual-emission properties were absent in the amine-free ppy and pppy complexes, which only displayed a broad emission band in fluid solutions (Figure 2c,d), indicative of the crucial role of the amine groups in the dual-emissive complexes. Thus, the possible pH-dependence of the emission of $[Ir(ppy\text{-}C4)_2(bpy\text{-}Et)](PF_6)$ was studied. We found that the emission intensity of the complex was strongly dependent on the pH, with a maximum intensity at ca. pH 5 (Supporting Information Figure S2). Both increasing and decreasing the pH value led to emission quenching. Importantly, the emission profile of the complex was independent of the pH. Thus, the dual-emission properties of the complex should not result from the different protonated situations of the amino groups. The broad emission bands of the two amine-free ppy and pppy complexes occurred at a similar wavelength to the LE emission of the dual-emissive complexes, and their origins were assigned to a $^3$CT state. This assignment is supported by the fact that the pppy complex (598 nm) emitted at a shorter wavelength than the ppy complex (609 nm) in $CH_2Cl_2$ (Table 1), as a result of the electron-withdrawing property of the phenyl substituent of the cyclometalating ligand. Interestingly, the $^3$CT emission band of the pppy-C4 complex occurred at a longer wavelength (602 nm) than that of the ppy-C4 complex (593 nm) in $CH_2Cl_2$ (Table 1), probably due to the presence of the electron-rich amino groups. The strong electron-donating ability of the amino groups may neutralize and even reverse the electron-withdrawing effect of the phenyl group.

To study the effects of diimine ligands, we selected four diimine ligands ($Me_4$-phen, $Me_2$-bpy, phen, $Ph_2$-phen) of different $\pi^*$ energy levels. Among the ppy-C4 complexes, complexes with the $Me_4$-phen and $Me_2$-bpy ligands (which are of higher-lying $\pi^*$ energy levels), i.e., $[Ir(ppy\text{-}C4)_2(N^N)](PF_6)$ (N^N = $Me_4$-phen, $Me_2$-bpy), displayed dual emission, which was similar to that of the bpy-Et complex (Figure 2e,f and Table 1). Changing the diimine ligands did not influence significantly the HE emission energy and lifetime, whereas the LE emission energy of the $Me_4$-phen complex was higher than that of the $Me_2$-bpy complex, which is in accordance with the $\pi$-accepting properties of the diimine ligands. These are consistent with the assignment of the HE emission to the $^3$IL ($\pi \rightarrow \pi^*$) (ppy-C4) excited state and the LE emission to the $^3$CT state associated with the $\pi^*$(N^N) orbital. Upon lowering the $\pi^*$ energy level of the diimine ligand, the dual emission feature became less noticeable; for example, the phen complex $[Ir(ppy\text{-}C4)_2(phen)](PF_6)$ only showed a broad LE band in $CH_2Cl_2$ and $CH_3CN$, and an additional weak HE shoulder also appeared at ca. 480 nm ($\tau_o$ = 2.92 $\mu$s) in aqueous buffer (Table 1 and Supporting Information Figure S3). The $Ph_2$-phen complex $[Ir(ppy\text{-}C4)_2(Ph_2\text{-}phen)](PF_6)$ did not show dual emission in fluid solutions at all and only exhibited an LE band at ca. 577−580 nm (Table 1 and Supporting Information Figure S4).

The emission properties of the four pppy-C4 complexes $[Ir(pppy\text{-}C4)_2(N^N)](PF_6)$ (N^N = $Me_4$-phen, $Me_2$-bpy, phen, $Ph_2$-phen) were similar to those of their corresponding ppy-C4 counterparts (Table 1). For the dual-emissive $Me_4$-phen and $Me_2$-bpy complexes, the additional phenyl ring in the cyclometalating ligand lowered the emission energy of the HE bands, which was also observed in the case of the bpy-Et complexes. As a result, the HE and LE emission bands of these two complexes were not well-resolved (Supporting Information Figures S5 and S6). Similar to their ppy-C4 counterparts, the dual emission of the phen complex $[Ir(pppy\text{-}C4)_2(phen)](PF_6)$ was only observed in aqueous solution (Supporting Information Figure S7), and the $Ph_2$-phen complex $[Ir(pppy\text{-}C4)_2(Ph_2\text{-}phen)](PF_6)$ exhibited only a broad emission band (Supporting Information Figure S8) in all the solvents we used. As expected, the amine-free pppy complexes $[Ir(pppy)_2(N^N)](PF_6)$ (N^N = $Me_4$-phen, $Me_2$-bpy, phen, $Ph_2$-phen) displayed a single emission band in fluid solutions (Table 1), which was assigned to a mixed $^3$MLCT ($d\pi(Ir) \rightarrow \pi^*$(N^N)) and $^3$LLCT ($\pi$(pppy) $\rightarrow \pi^*$(N^N)) excited state. The $Me_4$-phen and $Me_2$-bpy complexes showed structured emission bands,


DOI: 10.1021/acs.inorgchem.5b00944
Inorg. Chem. XXXX, XXX, XXX−XXX

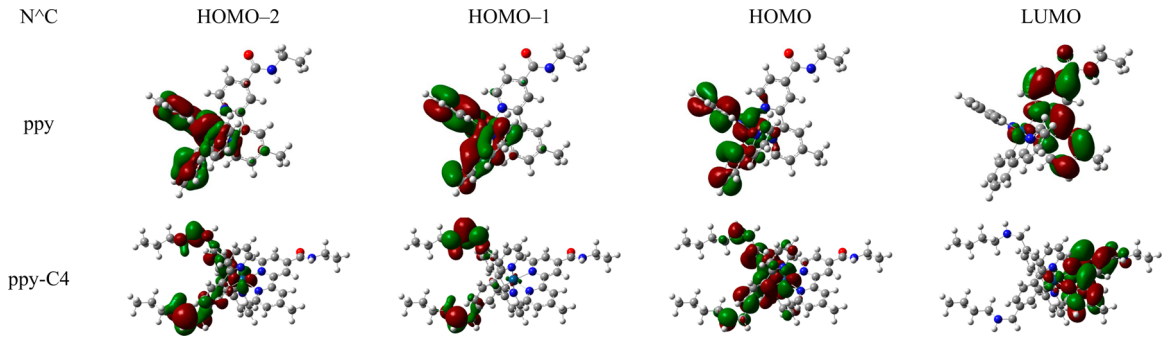


**Figure 3.** Molecular orbitals (isosurface plots) of $[Ir(N^C)_2(bpy\text{-}Et)](PF_6)$ (N^C = ppy, ppy-C4).

**Table 2. Calculated Triplet Transitions and the Frontier Orbitals of $[Ir(N^C)_2(bpy\text{-}Et)](PF_6)$ (N^C = ppy, ppy-C4)**

| complex | state | energy/eV (nm) | molecular orbital | main transition character |
|---|---|---|---|---|
| $[Ir(ppy)_2(bpy\text{-}Et)](PF_6)$ | T1 | 2.16 (574.9) | HOMO → LUMO (100%) | $ML_{bpy\text{-}Et}CT + L_{ppy}L_{bpy\text{-}Et}CT$ |
| | T2 | 2.64 (469.6) | HOMO − 2 → LUMO (65%) | $ML_{bpy\text{-}Et}CT + L_{ppy}L_{bpy\text{-}Et}CT$ |
| | | | HOMO − 4 → LUMO (13.9%) | |
| | T3 | 2.69 (460.6) | HOMO → LUMO + 2 (56.6%) | $ML_{ppy}CT + IL_{ppy}$ |
| | | | HOMO − 1 → LUMO + 3 (17.3%) | |
| | T4 | 2.70 (459.7) | HOMO − 1 → LUMO (47.6%) | $ML_{bpy\text{-}Et}CT + L_{ppy}L_{bpy\text{-}Et}CT$ |
| | | | HOMO − 3 → LUMO (34.9%) | |
| | T5 | 2.73 (454.0) | HOMO → LUMO + 3 (62.2%) | $ML_{ppy}CT + IL_{ppy}$ |
| | | | HOMO − 1 → LUMO + 2 (26.8%) | |
| $[Ir(ppy\text{-}C4)_2(bpy\text{-}Et)](PF_6)$ | T1 | 2.08 (596.3) | HOMO → LUMO (83.4%) | $ML_{bpy\text{-}Et}CT + L_{ppy}L_{bpy\text{-}Et}CT + N_{amine}L_{bpy\text{-}Et}CT$ |
| | | | HOMO − 2 → LUMO (16.6%) | |
| | T2 | 2.50 (495.0) | HOMO − 1 → LUMO (67.7%) | $N_{amine}L_{bpy\text{-}Et}CT$ |
| | | | HOMO − 2 → LUMO (22.3%) | |
| | T3 | 2.53 (489.8) | HOMO − 2 → LUMO (57.4%) | $N_{amine}L_{bpy\text{-}Et}CT$ |
| | | | HOMO − 1 → LUMO (32.3%) | |
| | T4 | 2.61 (475.1) | HOMO − 6 → LUMO (30.4%) | $ML_{bpy\text{-}Et}CT + L_{ppy}L_{bpy\text{-}Et}CT$ |
| | | | HOMO − 3 → LUMO (24.6%) | |
| | T5 | 2.65 (468.3) | HOMO − 3 → LUMO (27.8%) | $ML_{bpy\text{-}Et}CT + L_{ppy}L_{bpy\text{-}Et}CT + ML_{ppy}CT$ |
| | | | HOMO − 5 → LUMO (27.3%) | |
| | T6 | 2.65 (467.5) | HOMO → LUMO + 2 (56.8%) | $ML_{ppy}CT + IL_{ppy}$ |
| | | | HOMO − 3 → LUMO + 3 (16.7%) | |
| | T7 | 2.68 (462.1) | HOMO → LUMO + 3 (53.3%) | $ML_{ppy}CT + IL_{ppy}$ |
| | | | HOMO − 3 → LUMO + 2 (29.4%) | |

suggesting that their emissive states may also possess some $^3IL$ ($\pi \rightarrow \pi^*$) (N^N) character.

To develop luminescent bioprobes with dual-emissive properties, we incorporated a biotin moiety into the diimine ligand and prepared the complexes $[Ir(N^C)_2(bpy\text{-}biotin)](PF_6)$ (N^C = ppy-C4, pppy-C4, pppy). As expected, the amine-containing ppy-C4 and pppy-C4 complexes showed dual emission in fluid solutions (Table 1 and Figure 2g,h), and the amine-free pppy complex only displayed a single broad emission band. Since the addition of a biotin moiety does not significantly affect the electronic structure of the bipyridine unit, the emission behavior of these biotin complexes was very similar to that of the bpy-Et complexes (Table 1).

Taken together, we can conclude that only the amine-containing complexes exhibited dual emission. The HE $^3IL$ ($\pi \rightarrow \pi^*$) (N^C) state was more sensitive to the modification of the cyclometalating ligand. Also, changing the diimine ligands can tune the energy of the LE $^3CT$ state. Interestingly, when the $\pi^*$ levels of the diimine ligands are too low in energy, single LE $^3CT$ emission bands were observed as a consequence of the improved communication between the HE and the LE states.

**Theoretical Calculations.** To gain more insight into the nature of the excited states, TD-DFT calculations have been performed on $[Ir(N^C)_2(bpy\text{-}Et)](PF_6)$ (N^C = ppy, ppy-C4). The molecular orbitals (isosurface plots) of both complexes are shown in Figure 3 and Supporting Information Figure S8. The triplet transitions and frontier orbitals are listed in Table 2. The HOMO and the nearby occupied MO of both complexes were mainly localized at the iridium(III) center and the cyclometalating ligands, which is commonly observed in bis-cyclometalated iridium(III) diimine complexes.[47−50] Importantly, the secondary amines in $[Ir(ppy\text{-}C4)_2(bpy\text{-}Et)](PF_6)$ were also involved in these orbitals, especially in HOMO − 1 and HOMO − 2 (Figure 3). The LUMO and LUMO + 1 of both complexes were primarily on the bipyridine ligand including the substituted amide group, whereas LUMO + 2 and LUMO + 3 were mainly localized on the phenylpyridine ligands (Supporting Information Figure S9). The calculated excited states of both complexes were generally similar (Table 2); for example, the lowest-energy triplet excited states $T_1$ of $[Ir(ppy)_2(bpy\text{-}Et)](PF_6)$ and $[Ir(ppy\text{-}C4)_2(bpy\text{-}Et)](PF_6)$ occurred at 2.16 and 2.08 eV (574.9 and 596.3 nm), respectively, and were mainly composed of $ML_{bpy\text{-}Et}CT$ and $L_{ppy}L_{bpy\text{-}Et}CT$


DOI: 10.1021/acs.inorgchem.5b00944
Inorg. Chem. XXXX, XXX, XXX−XXX

transitions, with a small extent of $N_{amine}L_{bpy\text{-}Et}CT$ character in the ppy-C4 complex. Thus, these states of highly mixed nature are best described as $^3CT$ states. The second lowest-energy state of $[Ir(ppy)_2(bpy\text{-}Et)](PF_6)$ degenerated into T2−T5 (2.64−2.73 eV, 469.6−454.0 nm), between which the energy difference was as small as 0.09 eV (Table 2). The ppy-C4 complex $[Ir(ppy\text{-}C4)_2(bpy\text{-}Et)](PF_6)$ also showed very similar degenerated states T4−T7, composed of transitions of basically the same origins, at 2.61−2.68 eV (475.1−462.1 nm) (Table 2). Although these states are admixtures of $ML_{bpy\text{-}Et}CT$, $ML_{ppy}CT$, $L_{ppy}L_{bpy\text{-}Et}CT$, and $IL_{ppy}$ transitions, the IL character should be highlighted due to the distinctive photophysical properties (long lifetime and structural features) of the HE band. The most significant difference between the two complexes is that $[Ir(ppy\text{-}C4)_2(bpy\text{-}Et)](PF_6)$ exhibited an additional $N_{amine}L_{bpy\text{-}Et}CT$ transition (T2 and T3) occurring at 2.50−2.53 eV (495.0−489.8 nm), which originates from HOMO − 1 and HOMO − 2 to LUMO (Table 2). Since these states are absent in the ppy complex, they should play a crucial role in the interesting dual-emission properties of the amine-containing ppy-C4 complexes. On the basis of the above experimental and theoretical information, we propose orbital energy diagrams for the two complexes (Figure 4). On the basis

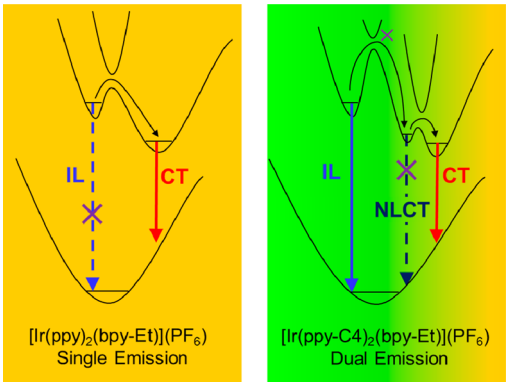


**Figure 4.** Proposed orbital energy diagrams of $[Ir(N^C)_2(bpy\text{-}Et)](PF_6)$ (N^C = ppy, ppy-C4).

of their excited-state nature, the degenerated frontier states and the lowest-energy triplet excited states are denoted as $T_{IL}$ and $T_{CT}$, respectively. The excited ppy complex $[Ir(ppy)_2(bpy\text{-}Et)](PF_6)$ undergoes efficient internal conversion from the $T_{IL}$ to the lowest-lying emissive $T_{CT}$ state, leading to the exclusive LE emission with predominant $^3CT$ character (Figure 4). In contrast, in the case of the ppy-C4 complex $[Ir(ppy\text{-}C4)_2(bpy\text{-}Et)](PF_6)$, the additional $T_{NLCT}$ state interrupts the communication between the two states $T_{IL}$ and $T_{CT}$. Also, it is likely that the additional energy barrier between the $T_{IL}$ and $T_{NLCT}$ states limits efficient internal conversion, resulting in dual emission from both triplet excited states. We believe that the existence of the $T_{NLCT}$ state is essential to the dual-emissive properties of these complexes.

**Utilization of Dual-Emissive Complexes as Ratiometric Probes.** During the investigation of the emission properties of these iridium(III) complexes, we found that the complexes exhibited ratiometric emissive response toward the polarity of solvents under deaerated conditions (Table 1 and Figure 2). To extend the applications of these complexes as ratiometric probes for other analytes, biotin was incorporated into the dual-emissive system to afford potential ratiometric probes for avidin. Biotin binds to the glycoprotein avidin with an extremely high affinity, and the biotin−avidin system has been widely utilized as a powerful tool in bioanalytical applications.[51] The 4′-hydroxyazobenzene-2-carboxylic acid (HABA) assay, which is based on the competition between biotin and HABA on binding to avidin,[52] confirmed that the biotin moiety in the complexes $[Ir(N^C)_2(bpy\text{-}biotin)](PF_6)$ (N^C = ppy-C4, pppy-C4, pppy) maintained avidin-binding affinity. Addition of the biotin complexes to a mixture of avidin and HABA led to a decrease in absorbance at 500 nm, indicating that the biotin moieties of the complexes can displace the avidin-bound HABA molecules (Supporting Information Figure S10). Also, the avidin-binding properties of the complexes were studied by emission titrations. The dual-emissive complexes $[Ir(N^C)_2(bpy\text{-}biotin)](PF_6)$ (N^C = ppy-C4, pppy-C4) showed a decrease in the HE band intensity and an increase in LE band intensity in aerated buffer, resulting in clear isoemissive points at 574 and 529 nm, respectively (Figure 5a,b). The ratiometric response became more significant when

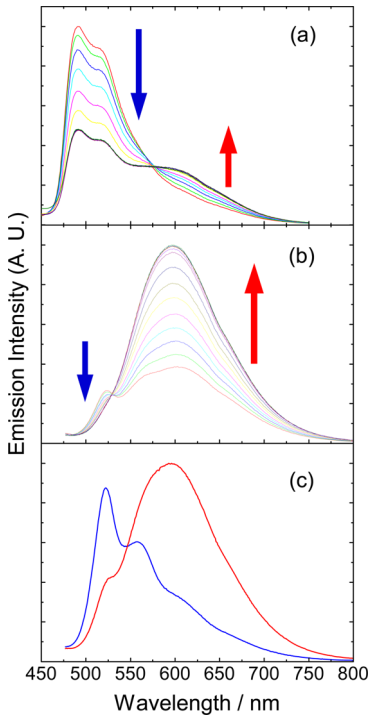


**Figure 5.** Emission spectral traces of $[Ir(N^C)_2(bpy\text{-}biotin)](PF_6)$ (N^C = ppy-C4 (a), pppy-C4 (b)) (10 $\mu$M) in aerated potassium phosphate buffer (50 mM, pH 7.4)/$CH_3OH$ (9:1, v/v) at 298 K upon addition of avidin. (c) Emission spectra of $[Ir(pppy\text{-}C4)_2(bpy\text{-}biotin)](PF_6)$ (10 $\mu$M) in the absence (blue) and presence (red) of avidin (2.5 $\mu$M) in degassed potassium phosphate buffer (50 mM, pH 7.4)/$CH_3OH$ (9:1, v/v) at 298 K.

the titration was performed in deaerated solutions because the HE emission was more intense in the absence of oxygen (Figure 5c). In view of the solvent-dependent emission of the ppy-C4 and pppy-C4 biotin complexes, we attributed the changes of emission profile of both complexes to the increased hydrophobicity of the local environment of the complexes upon binding to avidin.[45] For comparison, $[Ir(pppy)_2(bpy\text{-}biotin)](PF_6)$ only displayed a broad band ca. 599 nm in aqueous buffer, and showed emission enhancement without a shift in wavelength in response to avidin binding (Supporting


DOI: 10.1021/acs.inorgchem.5b00944
Inorg. Chem. XXXX, XXX, XXX−XXX

Information Figure S11). Similar observations have been commonly observed in luminescent transition metal biotin complexes developed in this laboratory.[53−55] It is noteworthy that the possibility of using these dual-emissive complexes as bioprobes is basically unlimited. We believe that the incorporation of other biological substrates or molecular/ion recognition units into this system will lead to new ratiometric probes that will display pronounced changes in their emission profile and spectral characteristics upon interaction with the protein hosts or analyte molecules/ions.[45]

**Cellular Uptake Efficiency and Cytotoxicity.** The cellular uptake efficiency of all the complexes was analyzed by ICP-MS. Generally speaking, it is well-known that more lipophilic complexes usually exhibit a higher diffusion rate through the cell membrane.[44] In this work, an average HeLa cell incubated with the complexes (2 $\mu$M, 2 h, 37 °C) contained 0.54−5.82 fmol of iridium (Table 3). It is reasonable that the

**Table 3. Numbers of Moles of Iridium Associated with an Average HeLa Cell upon Incubation with the Iridium(III) Complexes (2 $\mu$M) at 37 °C for 2 h As Determined by ICP-MS**

| complex | N^N | Ir/fmol |
|---|---|---|
| $[Ir(ppy\text{-}C4)_2(N^N)](PF_6)$ | bpy-Et | 0.59 ± 0.05 |
| | bpy-biotin | 0.54 ± 0.03 |
| | $Me_4$-phen | 0.66 ± 0.09 |
| | $Me_2$-bpy | 0.72 ± 0.10 |
| | phen | 0.74 ± 0.10 |
| | $Ph_2$-phen | 0.77 ± 0.12 |
| $[Ir(pppy\text{-}C4)_2(N^N)](PF_6)$ | bpy-Et | 1.34 ± 0.19 |
| | bpy-biotin | 1.04 ± 0.15 |
| | $Me_4$-phen | 5.24 ± 0.43 |
| | $Me_2$-bpy | 5.20 ± 0.47 |
| | phen | 4.91 ± 0.38 |
| | $Ph_2$-phen | 5.60 ± 0.55 |
| $[Ir(pppy)_2(N^N)](PF_6)$ | bpy-Et | 3.91 ± 0.40 |
| | bpy-biotin | 2.99 ± 0.23 |
| | $Me_4$-phen | 5.55 ± 0.62 |
| | $Me_2$-bpy | 5.51 ± 0.49 |
| | phen | 5.44 ± 0.50 |
| | $Ph_2$-phen | 5.82 ± 0.73 |

less lipophilic ppy-C4 complexes exhibited lower cellular uptake efficiency (0.54−0.77 fmol) than their pppy-C4 (1.04−5.60 fmol) and pppy (2.99−5.82 fmol) counterparts. Also, the pppy-C4 complexes, especially those with the bpy-Et and bpy-biotin ligands, showed lower uptake efficiency than their pppy counterparts, which is apparently a result of the polar amine groups in the *n*-butylaminomethyl substituents. Additionally, the complexes with the polar biotin unit $[Ir(N^C)_2(bpy\text{-}biotin)](PF_6)$ (N^C = ppy-C4, pppy-C4, pppy) showed the lowest uptake efficiency among all the complexes.

The cytotoxic activity of the complexes was evaluated by the MTT assay.[56] HeLa cells treated with the complexes (10 $\mu$M) for 12 h at 37 °C maintained >98% viability. Despite this cellular viability, the possibility of early apoptosis induced by the presence of the complexes cannot be excluded; this was examined using the Annexin V assay.[57] HeLa cells were pretreated with the complexes (10 $\mu$M, 12 h, 37 °C) and then incubated with the Annexin V-AlexaFluor 647 conjugate. Upon excitation at 633 nm (where the complexes do not absorb), the cells treated with the complexes $[Ir(N^C)_2(N^N)](PF_6)$ (N^C = pppy-C4, pppy; N^N = $Me_4$-phen, $Me_2$-bpy, phen, $Ph_2$-phen), which showed relatively high uptake efficiency, exhibited intense emission from the peripheral cell membrane. As an example, the confocal microscopy image of the cells treated with $[Ir(pppy)_2(Me_4\text{-phen})](PF_6)$ is shown in Figure 6a. Since

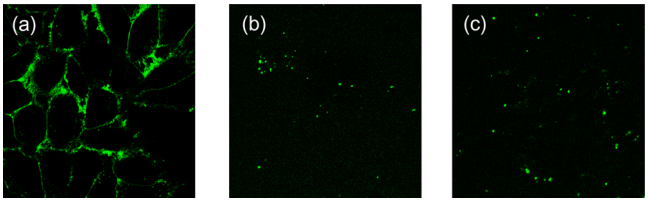


**Figure 6.** Confocal microscopy images of HeLa cells pretreated with $[Ir(pppy)_2(Me_4\text{-phen})](PF_6)$ (10 $\mu$M) (a), $[Ir(ppy\text{-}C4)_2(bpy\text{-}biotin)](PF_6)$ (10 $\mu$M) (b), and no complex (c) at 37 °C for 12 h and then incubated with the Annexin V, Alexa Fluor 647 conjugate (50 $\mu$L/mL) at 25 °C for 15 min.

Annexin V only stains cells that express phosphatidylserine on the cell surface, which is a characteristic of apoptosis,[57] the results indicate that these complexes caused apoptotic cell death. Interestingly, the cells treated with the other complexes including the ppy-C4, bpy-Et, and bpy-biotin complexes (10 $\mu$M, 12 h, 37 °C) showed much weaker emission (Figure 6b), which was similar to the untreated cells (Figure 6c), indicating that these complexes did not cause apoptotic cell death under these conditions.

**Intracellular Localization Studies.** The intracellular localization of all the complexes was investigated using laser-scanning confocal microscopy. It is important and necessary to employ a suitable condition under which the complexes give good-quality images with minimum cell death. Thus, we incubated HeLa cells with the complexes at a concentration of 0.5−5 $\mu$M for 1−6 h and traced the possible early apoptosis using the Annexin V assay. Either lowering the complex concentration or shortening the incubation duration significantly reduced the peripheral membrane staining by the Annexin V-Alexa Fluor conjugate (Supporting Information Figure S12). When HeLa cells were incubated with $[Ir(pppy)_2(Me_4\text{-phen})](PF_6)$ at a concentration lower than 3 $\mu$M for less than 3 h, the confocal microscopy images ($\lambda_{ex}$ = 633 nm) displayed similar emission intensity compared to those of the untreated cells, indicating that no apoptosis occurred. Thus, we selected a complex concentration of 2 $\mu$M and an incubation period of 2 h for our imaging studies.

HeLa cells treated with the complexes at 37 °C for 2 h revealed intense emission. Interestingly, the intracellular localization of these complexes was very different (Figure 7).

On the basis of the observations, the complexes were put into three groups. Group I includes the most lipophilic complexes such as the pppy complexes $[Ir(pppy)_2(N^N)](PF_6)$ (N^N = $Me_4$-phen, $Me_2$-bpy, phen, $Ph_2$-phen, bpy-Et, bpy-biotin) and the $Ph_2$-phen complexes $[Ir(N^C)_2(Ph_2\text{-phen})](PF_6)$ (N^C = ppy-C4, pppy-C4). Similar to most iridium(III) complexes, they were readily internalized and localized in the perinuclear region of cells. Group II includes complexes of medium lipophilicity, including $[Ir(N^C)_2(N^N)](PF_6)$ (N^C = ppy-C4, pppy-C4; N^N = $Me_2$-bpy, phen, $Me_4$-phen). Cells incubated with these complexes displayed two sharp luminescent rings; the interior one was around the nuclei while the exterior one surrounded the whole cell. Group III includes the least lipophilic *n*-butylaminomethyl


DOI: 10.1021/acs.inorgchem.5b00944
Inorg. Chem. XXXX, XXX, XXX−XXX

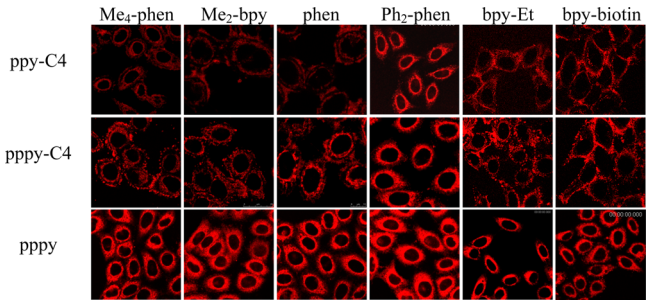


**Figure 7.** Confocal microscopy images of HeLa cells incubated with 2 $\mu$M of $[Ir(N^C)_2(N^N)](PF_6)$ (N^C = ppy-C4, pppy-C4, pppy; N^N = $Me_4$-phen, $Me_2$-bpy, phen, $Ph_2$-phen, bpy-Et, bpy-biotin) at 37 °C for 2 h. The emission at 570 ± 50 nm was collected.

complexes with the polar amide-substituted bipyridine ligands bpy-Et and bpy-biotin $[Ir(N^C)_2(N^N)](PF_6)$ (N^C = ppy-C4, pppy-C4; N^N = bpy-Et, bpy-biotin). HeLa cells stained by these complexes revealed intense emission on their cell surface, while the cytoplasm was much less emissive.

To determine the intracellular localization of these complexes, we co-stained live HeLa cells with the complexes and the fluorescent dye MitoTracker Deep Red FM. The Group I complex $[Ir(pppy)_2(Ph_2\text{-phen})](PF_6)$ was significantly co-localized with MitoTracker, resulting in a co-localization coefficient (CC) of 97%, which confirmed that this complex was localized in the mitochondria of the cells (Figure 8a). High-

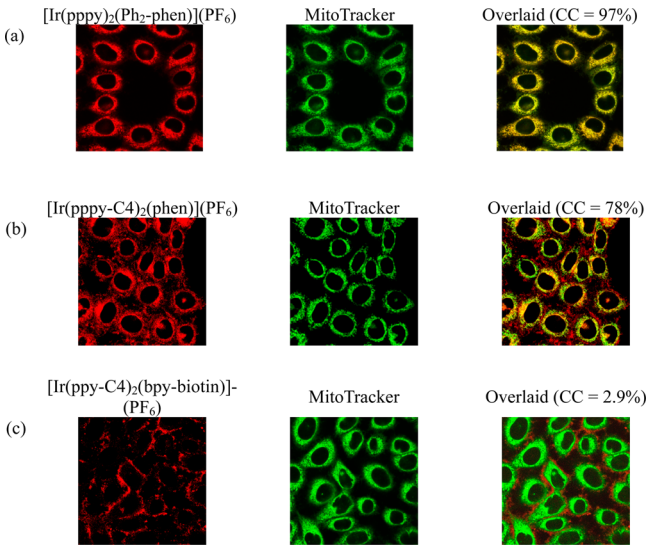


**Figure 8.** Confocal microscopy images of HeLa cells co-stained by the complexes and fluorescent dyes. Co-localization coefficients (CCs) are indicated in the overlaid images. The emission at 570 ± 50 and 670 ± 20 nm was collected for the complexes and fluorescent dyes, respectively.

quality mitochondria staining images can be obtained using a diluted solution of the complex and shorter incubation duration; for example, cells treated with $[Ir(pppy)_2(Me_4\text{-phen})](PF_6)$ at 0.3 $\mu$M for 30 min showed specific mitochondrial staining with a fairly high CC of 88% with MitoTracker (Supporting Information Figure S13). The Group II complex $[Ir(pppy\text{-}C4)_2(phen)](PF_6)$ was partially co-localized with MitoTracker, revealing a CC of 78% (Figure 8b). It can be seen in the overlaid image that co-staining occurred at the interior luminescent ring. The Group III complex $[Ir(ppy\text{-}C4)_2(bpy\text{-biotin})](PF_6)$ was hardly co-localized with MitoTracker (CC = 2.9%, Figure 8c). All these confocal microscopy images can be interpreted as follows: the most lipophilic pppy and $Ph_2$-phen complexes exhibited the most efficient internalization and subsequent localization at the mitochondria. However, the amine-containing ppy-C4 and pppy-C4 complexes were localized on the cell membrane or migrate into mitochondria, depending on their diimine ligands: (1) those complexes with the polar amide-substituted bipyridine ligands almost resided exclusively on the cell membrane; (2) those with the less polar ligands $Me_2$-bpy, phen, and $Me_4$-phen stained both the cell membrane and the mitochondria, giving rise to two luminescent rings. These results clearly indicate the importance of the lipophilicity of the complexes on their cellular staining properties. Interestingly, this structure-dependent intracellular distribution was only restricted to live cells since paraformaldehyde-fixed cells treated with the complexes showed indistinguishable staining behavior (Supporting Information Figure S14). Basically, the fixed cells displayed intense emission evenly in the cytoplasm and less intense emission in the nuclei. Thus, the membrane-staining properties of Groups II and III complexes were a consequence of limited uptake and suppression of further internalization by live cells.

## CONCLUSION

In this work, we systematically varied the cyclometalating and diimine ligands to investigate the effects of the structures of the iridium(III) polypyridine complexes $[Ir(N^C)_2(N^N)](PF_6)$ on their emission properties. Remarkably, complexes with a secondary amine on the cyclometalating ligands ppy-C4 and pppy-C4 showed interesting dual emission. Photophysical and TD-DFT calculations revealed that such a property resulted from the interruption of the internal conversion from the $^3$IL to the $^3$CT state by an additional NLCT state. As a consequence, the emission profile of the complexes strongly depended on their coordinating ligands and their local environment. We demonstrated the application of the dual-emissive biotin complexes as ratiometric sensors for avidin. Additionally, all the complexes exhibited efficient uptake by live HeLa cells. Laser-scanning confocal microscopy revealed that the complexes were localized on the cell membrane, mitochondria, or both, depending on the nature of the substituents of the ligands. The results of this work can contribute to the future development of dual-emissive transition metal complexes as ratiometric probes and organelle-selective bioimaging reagents.

## EXPERIMENTAL SECTION

**Materials and Synthesis.** All solvents were of analytical reagent grade and purified according to standard procedures.[58] All buffer components were of biological grade and used as received. $IrCl_3 \cdot 3H_2O$, Hppy-CHO, diethylamine, triethylamine, *n*-butylamine, triphenylphosphine, and $Pd(PPh_3)_2Cl_2$ were purchased from Aldrich. *N*-Boc-1,6-diaminohexane hydrochloride was purchased from International Laboratory. Palladium(II) chloride, copper(I) iodide, DCC, NHS, $Na_2CO_3$, 4-bromoanilane, pyridine, $NaNO_2$, 4-formylphenylboronic acid, phenylboronic acid, phen, $Me_4$-phen, $Ph_2$-phen, $MgSO_4$, $NaBH_4$, ferrocene, $KPF_6$, and cisplatin were purchased from Acros. $Me_2$-bpy was obtained from BDH. HABA and MTT were purchased from Sigma. Avidin was purchased from Calbiochem. The diimine ligands bpy-Et and bpy-biotin, and $[Ir(ppy\text{-}C4)_2(N^N)](PF_6)$, were prepared according to reported procedures.[45] TBAP was obtained from Aldrich and was recrystallized from hot ethanol and dried *in*


DOI: 10.1021/acs.inorgchem.5b00944
*Inorg. Chem.* XXXX, XXX, XXX−XXX

*vacuo* at 110 °C before use. HeLa cells were obtained from American Type Culture Collection. DMEM, FBS, PBS, trypsin-EDTA, penicillin/streptomycin, MitoTracker Deep Red FM, and Annexin V, Alexa Fluor 647 conjugate were purchased from Invitrogen. The growth medium for cell culture contained DMEM with 10% FBS and 1% penicillin/streptomycin.

**Crystal Structure Determination of [Ir(ppy-C4)$_2$(Me$_2$-bpy)](PF$_6$).** Single crystals of the complex suitable for X-ray crystallographic studies were obtained by slow diffusion of petroleum ether (40−60 °C) vapor into a concentrated acetone solution of the complex. A crystal of dimensions 0.2 × 0.1 × 0.1 mm$^3$ mounted in a glass capillary was used for data collection at 28 °C on a MAR diffractometer with a 300 mm image plate detector using graphite monochromatized Mo K$\alpha$ radiation ($\lambda$ = 0.710 73 Å). Data collection was made with 1.5° oscillation steps of $\varphi$, 10 min exposure time, and a scanner distance at 120 mm. A total of 130 images were collected. The images were interpreted and intensity integrated using the program DENZO.[59] The structure was solved by direct methods employing the program SIR-97[60] on a PC. Iridium, phosphorus, and many non-hydrogen atoms were located according to the direct methods and the successive least-squares Fourier cycles. Positions of other non-hydrogen atoms were found after successful refinement by full-matrix least-squares using the program SHELXL-97.[61] One crystallographic asymmetric unit consists of half of a formula unit. In the final stage of least-squares refinement, all non-hydrogen atoms were refined anisotropically. Hydrogen atoms were generated by SHELXL-97. The positions of the hydrogen atoms were calculated on the basis of the riding mode with thermal parameters equal to 1.2 times that of the associated carbon atoms, and participated in the calculation of final *R*-indices. Crystal data and a summary of data collection and refinement details are given in Supporting Information Table S4.

**Physical Measurements and Instrumentation.** Equipment and procedures for the characterization and electrochemical and photophysical measurements have been described previously.[62] The details have been included in the Supporting Information. Luminescence quantum yields were measured by the optically dilute method[63] using an aerated aqueous solution of [Ru(bpy)$_3$]Cl$_2$ ($\Phi$ = 0.028) as the standard solution.[64]

**Computational Details.** The ground-state ($S_0$) structures of [Ir(N^C)$_2$(bpy-Et)](PF$_6$) (N^C = ppy, ppy-C4) have been optimized using density functional theory (DFT) with the B3LYP[65,66] hybrid functional. The LANL2DZ basis sets[67,68] are used for iridium and all other atoms. The quasirelativistic pseudopotential with 17 valence electrons for Ir atom is employed. This pseudopotential has been shown to give good agreements with experimental measurements.[47−50] Vibrational frequency calculations have been performed to verify the minimum nature of the optimized structures. On the basis of optimized geometries of the $S_0$ state, time-dependent (TD)-DFT calculations using the B3LYP functional and the same basis sets are carried out to obtain the vertical excitation energies of various triplet transitions.[69−71] The solvent effect of $CH_2Cl_2$ is taken into account by the polarized continuum model (PCM).[72,73] All calculations are done with the Gaussian 09 package of programs.[74]

**Emission Titrations.** In a typical experiment, aliquots (5 $\mu$L) of avidin (150 $\mu$M) in phosphate buffer (50 mM, pH 7.4) were added cumulatively to the iridium biotin complex (10 $\mu$M) in a mixture of the same buffer and MeOH (9:1, v/v) at 1 min intervals. The solution was excited at 350 nm, and the emission spectra were measured.

**ICP-MS.** HeLa cells were grown in a 60 mm tissue culture dish and incubated at 37 °C under a 5% $CO_2$ atmosphere for 48 h. The culture medium was removed and replaced with medium/DMSO (99:1, v/v) containing the complex (2 $\mu$M). After incubation for 2 h, the medium was removed, and the cell layer was washed gently with PBS (1 mL × 3). After that, the cell layer was trypsinized, digested in 65% $HNO_3$ (2 mL) at 70 °C for 2 h, and then diluted in Milli-Q water to the final volume of 10 mL for ICP-MS (PerkinElmer SCIEX, ELAN DRC Plus) analysis.

**MTT Assay.** The cytotoxic effect of the complexes toward HeLa cells was studied using the MTT assay. HeLa cells were seeded in a 96-well flat-bottomed microplate (10 000 cells/well) in growth medium (100 $\mu$L) and incubated at 37 °C under a 5% $CO_2$ atmosphere for 24 h. The iridium(III) complexes (10 $\mu$M) were then added to the wells in a mixture of growth medium/DMSO (99:1, v/v). Wells containing growth medium without cells were used as blank controls. The microplate was incubated at 37 °C under a 5% $CO_2$ atmosphere for 12 h. Then, 10 $\mu$L of MTT in PBS (5 mg mL$^{-1}$) was added to each well. The microplate was incubated at 37 °C under a 5% $CO_2$ atmosphere for another 4 h. Solubilization solution (100 $\mu$L) containing 10% SDS in 2-propanol/0.04 M HCl (1:1, v/v) was then added to each well, and the microplate was further incubated for 24 h. The absorbance of the solutions at 570 nm was measured with a SPECTRAmax 340 microplate reader (Molecular Devices Corp., Sunnyvale, CA). The cell viability of the complexes were calculated.

**Annexin V Assay.** The cell death process has been investigated using the Annexin V assay. HeLa cells were grown on a sterile glass coverslip in a 35 mm tissue culture dish and incubated at 37 °C under a 5% $CO_2$ atmosphere for 48 h. The culture medium was removed, and the cells were incubated with the complex in medium/DMSO (99:1, v/v). After that, the medium was removed, and the cell layer was washed gently with cold PBS (1 mL × 3). The cells were then incubated with the Annexin V, Alexa Fluor 647 conjugate (5 $\mu$L/100 $\mu$L) in the annexin-binding buffer (10 mM of HEPES, 140 mM of NaCl, and 2.5 mM of $CaCl_2$ pH 7.4) at room temperature for 15 min. After washing with the annexin-binding buffer (1 mL × 3), the coverslip was mounted onto slides for measurements. Imaging was performed using a confocal microscope (Leica TCS SPE) with an excitation wavelength at 633 nm. The emission at 670 ± 20 nm was collected.

**Confocal Microscopy.** HeLa cells were grown on a sterile glass coverslip in a 35 mm tissue culture dish and incubated at 37 °C under a 5% $CO_2$ atmosphere for 48 h. The culture medium was removed and replaced with medium/DMSO (99:1, v/v) containing the complex (2 $\mu$M). After incubation for 2 h, the medium was removed, and the cell layer was washed gently with PBS (1 mL × 3). The coverslip was mounted onto slides for measurements. Imaging was performed using a confocal microscope (Leica TCS SPE) with an excitation wavelength at 405 nm. The emission at 570 ± 50 nm was collected. In the co-localization experiments with MitoTracker, after being treated with complexes, the HeLa cells were incubated with MitoTracker Deep Red FM (100 nM) for 20 min and then washed with PBS (1 mL × 3). The co-localization coefficient was determined by ImageJ (Version 1.4.3.67).

## ■ ASSOCIATED CONTENT

### Ⓢ Supporting Information

Synthetic procedure, characterization data, and details of physical measurements and instrumentation; Table S1 summarizing the selected bond lengths (Å) and bond angles (deg) for [Ir(ppy-C4)$_2$(Me$_2$-bpy)](PF$_6$); Tables S2 and S3 summarizing the electronic absorption spectral data and electrochemical data, respectively; Table S4 summarizing the data collection and refinement details in the crystal structure determination; Figure S1 showing electronic absorption spectra; Figure S2 depicts the pH-dependent emission spectra of [Ir(ppy-C4)$_2$(bpy-Et)](PF$_6$); Figures S3−S8 displaying the emission spectra; Figure S9 indicating molecular orbitals obtained from TD-DFT calculations; Figure S10 showing results of HABA assays; Figure S11 displaying emission spectral traces of [Ir(pppy)$_2$(bpy-biotin)](PF$_6$) upon addition of avidin; Figures S12−S14 showing confocal images; and the CIF file for [Ir(ppy-C4)$_2$(Me$_2$-bpy)](PF$_6$) (CCDC 1058968). The Supporting Information is available free of charge on the ACS Publications website at DOI: 10.1021/acs.inorgchem.5b00944.

## ■ AUTHOR INFORMATION

### Corresponding Authors

*E-mail: iamyzhang@njupt.edu.cn.



DOI: 10.1021/acs.inorgchem.5b00944
*Inorg. Chem.* XXXX, XXX, XXX−XXX

*E-mail: bhkenlo@cityu.edu.hk.

### Notes

The authors declare no competing financial interest.

## ■ ACKNOWLEDGMENTS

The work described in this paper was supported by Nanjing University of Posts and Telecommunications (NY213097) and City University of Hong Kong (Project No. 9667090 and 7004210). K.K.-W.L. is grateful to the Croucher Foundation for the award of a Senior Research Fellowship.

## ■ REFERENCES

(1) Wysocki, L. M.; Lavis, L. D. *Curr. Opin. Chem. Biol.* **2011**, *15*, 752−759.
(2) Yuan, L.; Lin, W.; Zheng, K.; He, L.; Huang, W. *Chem. Soc. Rev.* **2013**, *42*, 622−661.
(3) Kaur, M.; Choi, D. H. *Chem. Soc. Rev.* **2015**, *44*, 58−77.
(4) Kim, H. N.; Ren, W. X.; Kim, J. S.; Yoon, J. *Chem. Soc. Rev.* **2012**, *41*, 3210−3244.
(5) Liu, Z.; He, W.; Guo, Z. *Chem. Soc. Rev.* **2013**, *42*, 1568−1600.
(6) Wang, X.-D.; Wolfbeis, O. S.; Meier, R. J. *Chem. Soc. Rev.* **2013**, *42*, 7834−7869.
(7) Li, S. P.-Y.; Lo, K. K.-W. *RSC Adv.* **2014**, *4*, 10560−10585.
(8) He, X.; Yam, V. W.-W. *Coord. Chem. Rev.* **2011**, *255*, 2111−2123.
(9) Zhao, Q.; Li, F.; Huang, C. *Chem. Soc. Rev.* **2010**, *39*, 3007−3030.
(10) Lo, K. K.-W.; Choi, A. W.-T.; Law, W. H.-T. *Dalton Trans.* **2012**, *41*, 6021−6047.
(11) Butler, S. J.; Parker, D. *Chem. Soc. Rev.* **2013**, *42*, 1652−1666.
(12) Somers, R. C.; Bawendi, M. G.; Nocera, D. G. *Chem. Soc. Rev.* **2007**, *36*, 579−591.
(13) Yao, J.; Yang, M.; Duan, Y. *Chem. Rev.* **2014**, *114*, 6130−6178.
(14) Yang, Y.; Zhao, Q.; Feng, W.; Li, F. *Chem. Rev.* **2013**, *113*, 192−270.
(15) Zhao, Q.; Huang, C.; Li, F. *Chem. Soc. Rev.* **2011**, *40*, 2508−2524.
(16) Xu, H.; Li, Q.; Wang, L.; He, Y.; Shi, J.; Tang, B.; Fan, C. *Chem. Soc. Rev.* **2014**, *43*, 2650−2661.
(17) Gai, S.; Li, C.; Yang, P.; Lin, J. *Chem. Rev.* **2014**, *114*, 2343−2389.
(18) Zhang, K. Y.; Li, S. P.-Y.; Zhu, N.; Or, I. W.-S.; Cheung, M. S.-H.; Lam, Y.-W.; Lo, K. K.-W. *Inorg. Chem.* **2010**, *49*, 2530−2540.
(19) Moromizato, S.; Hisamatsu, Y.; Suzuki, T.; Matsuo, Y.; Abe, R.; Aoki, S. *Inorg. Chem.* **2012**, *51*, 12697−12706.
(20) Nakagawa, A.; Hisamatsu, Y.; Moromizato, S.; Kohno, M.; Aoki, S. *Inorg. Chem.* **2014**, *53*, 409−422.
(21) Shang, L.; Stockmar, F.; Azadfar, N.; Nienhaus, G. U. *Angew. Chem., Int. Ed.* **2013**, *52*, 11154−11157.
(22) Papkovsky, D. B.; Dmitriev, R. I. *Chem. Soc. Rev.* **2013**, *42*, 8700−8732.
(23) Han, J.; Burgess, K. *Chem. Rev.* **2010**, *110*, 2709−2728.
(24) Sarkar, A. R.; Kang, D. E.; Kim, H. M.; Cho, B. R. *Inorg. Chem.* **2014**, *53*, 1794−1803.
(25) You, Y.; Lee, S.; Kim, T.; Ohkubo, K.; Chae, W. S.; Fukuzumi, S.; Jhon, G. J.; Nam, W.; Lippard, S. J. *J. Am. Chem. Soc.* **2011**, *133*, 18328−18342.
(26) Woo, H.; Cho, S.; Han, Y.; Chae, W. S.; Ahn, D. R.; You, Y.; Nam, W. *J. Am. Chem. Soc.* **2013**, *135*, 4771−4787.
(27) Hong-Hermesdorf, A.; Miethke, M.; Gallaher, S. D.; Kropat, J.; Dodani, S. C.; Chan, J.; Barupala, D.; Domaille, D. W.; Shirasaki, S. I.; Loo, J. A.; Weber, P. K.; Pett-Ridge, J.; Stemmler, T. L.; Chang, C. J.; Merchant, S. S. *Nat. Chem. Biol.* **2014**, *10*, 1034−1042.
(28) Lin, Q.; Bao, C.; Yang, Y.; Liang, Q.; Zhang, D.; Cheng, S.; Zhu, L. *Adv. Mater.* **2013**, *25*, 1981−1986.
(29) Lin, V. S.; Lippert, A. R.; Chang, C. J. *Proc. Natl. Acad. Sci. U.S.A.* **2013**, *110*, 7131−7135.
(30) Law, W. H.-T.; Leung, K.-K.; Lee, L. C.-C.; Poon, C.-S.; Liu, H.-W.; Lo, K. K.-W. *ChemMedChem* **2014**, *9*, 1316−1329.
(31) Choi, A. W.-T.; Yim, V. M.-W.; Liu, H.-W.; Lo, K. K.-W. *Chem.—Eur. J.* **2014**, *20*, 9633−9642.
(32) Yoshihara, T.; Yamaguchi, Y.; Hosaka, M.; Takeuchi, T.; Tobita, S. *Angew. Chem., Int. Ed.* **2012**, *51*, 4148−4151.
(33) Takahashi, S.; Piao, W.; Matsumura, Y.; Komatsu, T.; Ueno, T.; Terai, T.; Kamachi, T.; Kohno, M.; Nagano, T.; Hanaoka, K. *J. Am. Chem. Soc.* **2012**, *134*, 19588−19591.
(34) Huang, C.; Jia, T.; Tang, M.; Yin, Q.; Zhu, W.; Zhang, C.; Yang, Y.; Jia, N.; Xu, Y.; Qian, X. *J. Am. Chem. Soc.* **2014**, *136*, 14237−14244.
(35) Takei, Y.; Arai, S.; Murata, A.; Takabayashi, M.; Oyama, K.; Ishiwata, S.; Takeoka, S.; Suzuki, M. *ACS Nano* **2014**, *8*, 198−206.
(36) Zhang, K. Y.; Zhang, J.; Liu, Y.; Liu, S.; Zhang, P.; Zhao, Q.; Tang, Y.; Huang, W. *Chem. Sci.* **2015**, *6*, 301−307.
(37) Kasha, M. *Faraday Soc. Discuss.* **1950**, *9*, 14−19.
(38) Ladouceur, S.; Donato, L.; Romain, M.; Mudraboyina, B. P.; Johansen, M. B.; Wisner, J. A.; Zysman-Colman, E. *Dalton Trans.* **2013**, *42*, 8838−8847.
(39) Yeh, Y.-S.; Cheng, Y.-M.; Chou, P.-T.; Lee, G.-H.; Yang, C.-H.; Chi, Y.; Shu, C.-F.; Wang, C.-H. *ChemPhysChem* **2006**, *7*, 2294−2297.
(40) You, Y.; Han, Y.; Lee, Y.-M.; Park, S. Y.; Nam, W.; Lippard, S. J. *J. Am. Chem. Soc.* **2011**, *133*, 11488−11491.
(41) Thorp-Greenwood, F. L.; Fernández-Moreira, V.; Millet, C. O.; Williams, C. F.; Cable, J.; Court, J. B.; Hayes, A. J.; Lloyd, D.; Coogan, M. P. *Chem. Commun.* **2011**, *47*, 3096−3098.
(42) Zhou, Y.; Jia, J.; Li, W.; Fei, H.; Zhou, M. *Chem. Commun.* **2013**, *49*, 3230−3232.
(43) Sun, H.; Yang, L.; Yang, H.; Liu, S.; Xu, W.; Liu, X.; Tu, Z.; Su, H.; Zhao, Q.; Huang, W. *RSC Adv.* **2013**, *3*, 8766−8776.
(44) Zhang, K. Y.; Liu, S.; Zhao, Q.; Li, F.; Huang, W. *Struct. Bonding (Berlin)* **2014**, DOI: 10.1007/430_2014_166.
(45) Lo, K. K.-W.; Zhang, K. Y.; Leung, S.-K.; Tang, M.-C. *Angew. Chem., Int. Ed.* **2008**, *47*, 2213−2216.
(46) Miyaura, N.; Suzuki, A. *Chem. Rev.* **1979**, *95*, 2457−2483.
(47) Zhao, Q.; Cao, T.; Li, F.; Li, X.; Jing, H.; Yi, T.; Huang, C. *Organometallics* **2007**, *26*, 2077−2081.
(48) Avilov, I.; Minoofar, P.; Cornil, J.; De Cola, L. *J. Am. Chem. Soc.* **2007**, *129*, 8247−8258.
(49) Du, B.-S.; Lin, C.-H.; Chi, Y.; Hung, J.-Y.; Chung, M.-W.; Lin, T.-Y.; Lee, G.-H.; Wong, K.-T.; Chou, P.-T.; Hung, W.-Y.; Chiu, H.-C. *Inorg. Chem.* **2010**, *49*, 8713−8723.
(50) Li, X.-N.; Wu, Z.-J.; Li, X.-Y.; Zhang, H.-J.; Liu, X.-J. *J. Comput. Chem.* **2011**, *32*, 1033−1042.
(51) Wilchek, M.; Bayer, E. A. *Methods Enzymol.* **1990**, *184*, 123−138.
(52) Green, N. M. *Adv. Protein Chem.* **1975**, *29*, 85−133.
(53) Lo, K. K.-W.; Hui, W.-K.; Ng, D. C.-M. *J. Am. Chem. Soc.* **2002**, *124*, 9344−9345.
(54) Lo, K. K.-W.; Tsang, K. H.-K. *Organometallics* **2004**, *23*, 3062−3070.
(55) Lo, K. K.-W.; Tsang, K. H.-K.; Sze, K.-S. *Inorg. Chem.* **2006**, *45*, 1714−1722.
(56) Mosmann, T. J. *Immunol. Methods* **1983**, *65*, 55−63.
(57) van Engeland, M.; Nieland, L. J.; Ramaekers, F. C.; Schutte, B.; Reutelingsperger, C. P. *Cytometry* **1998**, *31*, 1−9.
(58) Perrin, D. D.; Armarego, W. L. F. *Purification of Laboratory Chemicals*; Pergamon: Oxford, 1997.
(59) Otwinowski, Z.; Minor, W. DENZO Program. In *Methods in Enzymology*; Academic Press: San Diego, CA, 1997; Vol. *276*, p 307−326.
(60) Altomare, A.; Burla, M. C.; Camalli, M.; Cascarano, G.; Giacovazzo, C.; Guagliardi, A.; Moliterni, A. G. G.; Polidori, G.; Spagna, R. *J. Appl. Crystallogr.* **1998**, *32*, 115−119.
(61) Sheldrick, G. M. *SHELXS-97 and SHELXL-97, Programs for Crystal Structure Analysis (Release 97−2)*; University of Göttingen: Göttingen, Germany, 1997.
(62) Zhang, K. Y.; Lo, K. K.-W. *Inorg. Chem.* **2009**, *48*, 6011−6025.
(63) Demas, J. N.; Crosby, G. A. *J. Phys. Chem.* **1971**, *75*, 991−1024.
(64) Nakamura, K. *Bull. Chem. Soc. Jpn.* **1982**, *55*, 2697−2705.
(65) Lee, C.; Yang, W.; Parr, R. G. *Phys. Rev. B* **1988**, *37*, 785−789.



DOI: 10.1021/acs.inorgchem.5b00944
*Inorg. Chem.* XXXX, XXX, XXX−XXX

(66) Becke, A. D. *J. Chem. Phys.* **1993**, *98*, 5648−5652.
(67) Hay, P. J.; Wadt, W. R. *J. Chem. Phys.* **1985**, *82*, 270−283.
(68) Hay, P. J.; Wadt, W. R. *J. Chem. Phys.* **1985**, *82*, 299−310.
(69) Autschbach, J.; Ziegler, T.; Gisbergen, S. J. A.; Baerends, E. J. *J. Chem. Phys.* **2002**, *116*, 6930−6940.
(70) Helgaker, T.; Jørgensen, P. *J. Chem. Phys.* **1991**, *95*, 2595−2601.
(71) Bak, K. L.; Jørgensen, P.; Helgaker, T.; Rund, K.; Jensen, H. J. A. *J. Chem. Phys.* **1993**, *98*, 8873−8887.
(72) Miertuš, S.; Scrocco, E.; Tomasi, J. *Chem. Phys.* **1981**, *55*, 117−129.
(73) Miertuš, S.; Tomasi, J. *Chem. Phys.* **1982**, *65*, 239−247.
(74) Frisch, M. J.; Trucks, G. W.; Schlegel, H. B.; Scuseria, G. E.; Robb, M. A.; Cheeseman, J. R.; Scalmani, G.; Barone, V.; Mennucci, B.; Petersson, G. A.; Nakatsuji, H.; Caricato, M.; Li, X.; Hratchian, H. P.; Izmaylov, A. F.; Bloino, J.; Zheng, G.; Sonnenberg, J. L.; Hada, M.; Ehara, M.; Toyota, K.; Fukuda, R.; Hasegawa, J.; Ishida, M.; Nakajima, T.; Honda, Y.; Kitao, O.; Nakai, H.; Vreven, T.; Montgomery, J. A., Jr.; Peralta, J. E.; Ogliaro, F.; Bearpark, M.; Heyd, J. J.; Brothers, E.; Kudin, K. N.; Staroverov, V. N.; Kobayashi, R.; Normand, J.; Raghavachari, K.; Rendell, A.; Burant, J. C.; Iyengar, S. S.; Tomasi, J.; Cossi, M.; Rega, N.; Millam, N. J.; Klene, M.; Knox, J. E.; Cross, J. B.; Bakken, V.; Adamo, C.; Jaramillo, J.; Gomperts, R.; Stratmann, R. E.; Yazyev, O.; Austin, A. J.; Cammi, R.; Pomelli, C.; Ochterski, J. W.; Martin, R. L.; Morokuma, K.; Zakrzewski, V. G.; Voth, G. A.; Salvador, P.; Dannenberg, J. J.; Dapprich, S.; Daniels, A. D.; Farkas, Ö.; Foresman, J. B.; Ortiz, J. V.; Cioslowski, J.; Fox, D. J. *Gaussian 09, Revision A.1*; Gaussian, Inc.: Wallingford, CT, 2009.


DOI: 10.1021/acs.inorgchem.5b00944
*Inorg. Chem.* XXXX, XXX, XXX−XXX